A LETTERS JOURNAL EXPLORING THE FRONTIERS OF PHYSICS

Società Italiana di Fisica
edp sciences
IOP Institute of Physics

LETTER

The evolution from BCS to Bose pairing in two-band superfluids: Quantum phase transitions and crossovers by tuning band offset and interactions

To cite this article: Yue-Ran Shi *et al* 2022 *EPL* **139** 36004 epl A Letters Journal Exploring the Frontiers of Physics

August 2022

EPL, **139** (2022) 36004
doi: 10.1209/0295-5075/ac8178

www.epljournal.org

The evolution from BCS to Bose pairing in two-band superfluids: Quantum phase transitions and crossovers by tuning band offset and interactions

Yue-Ran Shi[1,3], Wei Zhang[1,2(a)] and C. A. R. Sá de Melo[3(b)]

[1] *Department of Physics, Renmin University of China - Beijing 100872, China*
[2] *Beijing Key Laboratory of Opto-electronic Functional Materials and Micro-nano Devices, Renmin University of China - Beijing 100872, China*
[3] *School of Physics, Georgia Institute of Technology - Atlanta, GA 30332, USA*

received 17 May 2022; accepted in final form 15 July 2022
published online 8 August 2022

Abstract – We show that in two-band s-wave superfluids it is possible to induce quantum phase transitions (QPTs) by tuning intraband and interband s-wave interactions, in sharp contrast to single-band s-wave superfluids, where only a crossover between Bardeen-Cooper-Schrieffer (BCS) and Bose-Einstein condensation (BEC) superfluidity occurs. For non-zero interband and attractive intraband interactions, we demonstrate that the ground state has always two interpenetrating superfluids possessing three spectroscopically distinct regions where pairing is qualitatively different: I) BCS pairing in both bands (BCS-BCS), II) BCS pairing in one band and BEC pairing in the other (BCS-BEC), and III) Bose pairing in both bands (BEC-BEC). Furthermore, we show that by fine tuning the interband interactions to zero one can induce QPTs in the ground state between three distinct superfluid phases. There are two phases where only one band is superfluid (S_1 or S_2), and one phase where both bands are superfluid ($S_1 + S_2$), a situation which is absent in one-band s-wave systems. Lastly, we suggest that these crossovers and QPTs may be observed in multi-component systems such as ^{6}Li, ^{40}K, ^{87}Sr, and ^{173}Yb.

Introduction. – The evolution from Bardeen-Cooper-Schrieffer (BCS) to Bose pairing in one-band superfluids is a topic of intensive recent experimental [1–4], and theoretical [5–8] research, because it is the simplest system addressing the deep theoretical connection between BCS and Bose superfluidity [9–11] that arises in many areas of physics: condensed matter (superconductivity), atomic physics (ultracold Fermi superfluids), astrophysics (superfluid neutron stars) and quantum chromodynamics (color superconductivity) [12]. Although it is now possible to experimentally tune the carrier density in superconductors via gate voltages [13] or geometric configurations [14], the tunability of interactions is extremely limited or inexistent in quantum chromodynamics, astrophysics, and condensed matter physics. However, for low-density one-band Fermi atoms (^{6}Li or ^{40}K) it is possible to tune s-wave interactions and study the crossover from BCS to Bose-Einstein condensation (BEC) superfluidity [15–18], where large Cooper pairs evolve into tightly bound pairs, when interactions change from weak to strong.

Although the BCS-BEC crossover is interesting, its physics is not as striking as that occurring in quantum phase transitions (QPTs), where singular behavior emerges. In one-band superfluids, topological QPTs were theoretically predicted as a function of interaction strength for higher angular momentum pairing, such as p- or d-wave [19–22], leading to superfluid phases in the BCS and BEC regimes which are qualitatively different. However, the experimental observation of this phenomenon in cold gases has failed so far, because p-wave fermion pairs dissociate by tunneling out of the centrifugal barrier, that is, their lifetime is just not long enough to observe superfluidity [23–25]. This experimental fact, makes it currently impossible to study predicted QPTs in the superfluid state of p-wave or higher angular momentum pairing [26] as a function of interactions in three-dimensional geometries. However, there are recent [27] and earlier [28] reports

(a)E-mail: wzhangl@ruc.edu.cn (corresponding author)
(b)E-mail: carlos.sademelo@physics.gatech.edu

of collisional-loss reduction in p-wave scattering for a quasi-one-dimensional geometry, thus suggesting the possibility of having relatively stable p-wave pairs, which could lead to the observation of QPTs in future experiments.

In this paper, we propose an alternative idea to study elusive QPTs between qualitatively different superfluid states during the BCS to BEC evolution: tune only s-wave interactions, but enlarge the Hilbert space of states to two bands with or without an energy offset [29]. The tuning of s-wave interactions creates stable fermion pairs, while the existence of two bands allows for the emergence of QPTs. Our work provides new insights into the evolution from BCS to BEC in two-band superfluids in addition to the analysis of Goldstone and Leggett modes [30], zero and finite temperature theory for the crossover from BCS pairing to two types of BECs [31], zero temperature condensate fraction and crossover diagrams [32], Ginzburg-Landau theory of shallow and deep bands [33], screening of pair fluctuations [34] and enhancement of critical temperature [35].

Experimental candidates include systems with four states, such as ^{6}Li and ^{40}K, where interactions may be tuned via magnetic Feshbach resonances [15–18], or ^{87}Sr [36,37] and ^{173}Yb [38,39], where interactions may be tuned via orbital Feshbach resonances [40,41]. We investigate a Fermi gas with two parabolic bands per spin label (four states) separated by a band offset ε_0, whose physical origin can be a quadratic Zeeman shift or a higher energy state of the trap (harmonic, box or painted). We allow for s-wave intraband and interband interactions, where the latter is described by pair tunneling J. The special case of $J = 0$, may be realized depending on symmetry conditions. For instance, consider the example of atoms having two internal atomic states with spin labels $(\uparrow, \downarrow)$ and center-of-mass (CM) wave functions with the symmetry of the ground and first excited state of a harmonic trapping potential with anisotropies to avoid degeneracies in the first excited state. In this case, the Josephson tunneling between bands is expected to be essentially zero, because of the orthogonality of the CM wave functions. The energy difference between the first excited and the ground states, plays the role of the band offset ε_0, which can be tuned by changing trap frequencies.

We find two types of crossovers and two types of QPTs. For non-zero J, the ground-state phase diagram always exhibits superfluidity in both bands for any chosen values of the intraband interactions. This means that there are no QPTs, but there are two crossovers. Typical crossover lines separate regions which are spectroscopically distinct with respect to their quasiparticle excitation spectrum: I) both bands have indirect gaps (BCS-BCS); II) one band has an indirect gap and the other has a direct gap (BCS-BEC); III) both bands have direct gaps (BEC-BEC). The first type of QPT is a 0-π phase transition, where the relative phases of the s-wave order parameters in the two bands changes from 0 ($J > 0$) to π ($J < 0$). However, the second type of QPT occurs for $J = 0$, and leads to three different ground states as intraband interactions are changed: a) two phases where only one band is superfluid (S_1 or S_2); and b) one phase where both bands are superfluid ($S_1 + S_2$). Thus, QPTs in two-band s-wave superfluids are found, rather than standard crossover physics in the evolution from BCS to BEC superfluidity. To characterize the QPTs, we investigate pair sizes and the coherence lengths, and show that they describe different concepts like in the single band case. We derive a Ginzburg-Landau fluctuation theory and show that the appropriate coherence length diverges when a QPT is crossed. We also characterize the QPTs thermodynamically by revealing the existence of discontinuities in the compressibility.

Hamiltonian. – To explore QPTs in two-band s-wave superfluids, we start from the Hamiltonian

$$H = \sum_{j\mathbf{k}s} \xi_j(\mathbf{k}) c^\dagger_{j\mathbf{k}s} c_{j\mathbf{k}s} + \sum_{ij\mathbf{k}\mathbf{k}'\mathbf{q}} V_{ij}(\mathbf{k}, \mathbf{k}') b^\dagger_{i\mathbf{k}\mathbf{q}} b_{j\mathbf{k}'\mathbf{q}}, \quad (1)$$

where pair operators $b_{j\mathbf{k}\mathbf{q}} = c_{j,-\mathbf{k}+\mathbf{q}/2,\downarrow} c_{j,\mathbf{k}+\mathbf{q}/2,\uparrow}$ are defined in terms of fermion operators $c_{j\mathbf{k}s}$ with band index $j = \{1, 2\}$, momentum $\mathbf{k}$ and spin label $s = \{\uparrow, \downarrow\}$. We work in three dimensions (3D) and choose units where $\hbar = k_B = 1$. The term $\xi_j(\mathbf{k}) = \varepsilon_j(\mathbf{k}) - \mu$ is the kinetic energy for band j with respect to the chemical potential μ, with $\varepsilon_j(\mathbf{k}) = \varepsilon_{j0} + \frac{\mathbf{k}^2}{2m_j}$, where m_j is the band mass. We choose $\varepsilon_{10} = 0$ and $\varepsilon_{20} = \varepsilon_0 > 0$, where ε_0 is the energy offset between the two bands, as shown in fig. 1: the solid blue line (solid red line) represents band 1 (band 2), and $E_{F_1} = k^2_{F_1}/2m_1$ ($E_{F_2} = k^2_{F_2}/2m_2$) is the Fermi energy with Fermi momentum k_{F_1} (k_{F_2}). In eq. (1), $V_{ij}(\mathbf{k}, \mathbf{k}')$ are intraband and interband interactions. The interactions are written in the separable form $V_{ij}(\mathbf{k}, \mathbf{k}') = V_{ij}\Gamma_i(\mathbf{k})\Gamma_j(\mathbf{k}')$, where $\Gamma_i(\mathbf{k}) = [1+\mathbf{k}^2/k^2_R]^{-1/2}$, with $k_R \sim R^{-1}$. Here, R is the interaction range in real space. The symmetry factors $\Gamma_i(\mathbf{k})$, $\Gamma_j(\mathbf{k})$ in $V_{ij}(\mathbf{k}, \mathbf{k}')$ represent s-wave intraband pairing interactions V_{11} in band 1, and V_{22} in band 2; while the interband interactions $V_{12} = V_{21} = -J$ are Josephson couplings, that is, there is a momentum space proximity effect, where superfluidity in one band can induce superfluidity in the other.

Physical picture. – The parameters of the Hamiltonian in eq. (1) are: masses m_1 and m_2, interactions $V_{11} = -|V_{11}|$, $V_{22} = -|V_{22}|$, and $V_{12} = V_{21} = -J$, band offset ε_0, and chemical potential μ fixing the total number of particles $N = N_1 + N_2$. Next, we set $m_1 = m_2 = m$, but the arguments presented are based on energetics and are also valid for $m_1 \neq m_2$ [29]. To compare interactions to Fermi energies E_{F_1} and E_{F_2}, we write the interaction energy scales $\lambda_1 = |V_{11}|N_1$, $\lambda_2 = |V_{22}|N_2$, and $\lambda_J = J\sqrt{N_1 N_2}$.

In fig. 1, Fermi energies E_{F_1} and E_{F_2} are compared to interaction energies λ_1 and λ_2. The Josephson energy scale λ_J, not shown in the figure, is considered to the smallest of

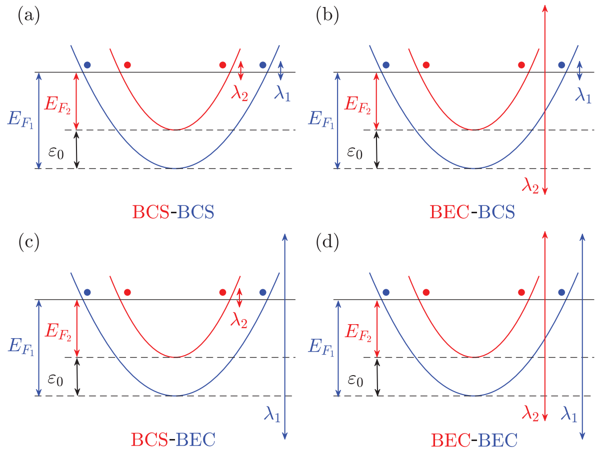

Fig. 1: Energy dispersions $\varepsilon_j(\mathbf{k})$ and Fermi energies E_{F_j} for $j = \{1, 2\}$: band 1 in blue is shifted down by ε_0 with respect to band 2 in red. Intraband interaction strengths are $\lambda_j = |V_{jj}|N_j$, where N_j is the number of particles in band j. When $\lambda_j \ll E_{F_j}$ ($\lambda_j \gg E_{F_j}$) pairing is BCS-like (BEC-like).

all. A simple analysis of these energy scales leads to four general outcomes. The first case is illustrated in panel (a), where the pairing energy scales $\lambda_1 \ll E_{F_1}$ and $\lambda_2 \ll E_{F_2}$ leading to BCS pairing in both bands (BCS-BCS), and pair sizes $\xi_1 \gg k_{F_1}^{-1}$ and $\xi_2 \gg k_{F_2}^{-1}$, where k_{F_j} is the Fermi momentum associated with band j. The second case is illustrated in panel (b), where $\lambda_1 \ll E_{F_1}$ and $\lambda_2 \gg E_{F_2}$ leading to BCS pairing in band 1 and BEC pairing in band 2 (BCS-BEC), and pair sizes $\xi_1 \gg k_{F_1}^{-1}$ and $\xi_2 \ll k_{F_2}^{-1}$. The third case is illustrated in panel (c), where $\lambda_1 \gg E_{F_1}$ and $\lambda_2 \ll E_{F_2}$ leading to BEC pairing in band 1 and BCS pairing in band 2 (BEC-BCS), and pair sizes $\xi_1 \ll k_{F_1}^{-1}$ and $\xi_2 \gg k_{F_2}^{-1}$. The fourth case is illustrated in panel (d), where $\lambda_1 \gg E_{F_1}$ and $\lambda_2 \gg E_{F_2}$ leading to BEC pairing in both bands (BEC-BEC), and pair sizes $\xi_1 \ll k_{F_1}^{-1}$ and $\xi_2 \ll k_{F_2}^{-1}$. The effect of λ_J is to transfer fermion pairs from one band to the other, thus guaranteeing that the ground state is always superfluid with both bands participating. Thus, when $\lambda_J \neq 0$, we can have only crossovers between the four regions. The case of $\lambda_J = 0$ is very special, because it blocks pair transfer, and allows for ground states where superfluidity exists not only in both bands, but also in just one band, as either interactions or band offset are changed. Thus, fine tuning λ_J to zero allows for QPT's between different superfluid phases rather than crossovers, even with only s-wave interactions.

Phase diagrams. – To obtain the thermodynamic potential $\Omega = -T \ln \mathcal{Z}$, where $\mathcal{Z}$ is the grand canonical partition function, we choose pairing to be independent of time and to occur at zero CM momentum ($\mathbf{q} = \mathbf{0}$), that is, the pairing field is $\Delta_j(\mathbf{q}) = \Delta_{j0}\delta_{\mathbf{q}\mathbf{0}}$, where Δ_{j0} is the order parameter for the j^{th} band. This approximation leads to $\Omega = \Omega_p + \Omega_c$. The first term is $\Omega_p = -\sum_{ij} \Delta_{i0}^* g_{ij} \Delta_{j0}$. The second term, arising from the fermionic degrees of freedom, is $\Omega_c = T\sum_{j\mathbf{k}} \left\{\beta\left[\xi_j(\mathbf{k}) - E_j(\mathbf{k})\right] - 2\ln\left[1 + e^{-\beta E_j(\mathbf{k})}\right]\right\}$, where the quasiparticle excitation energy is $E_j(\mathbf{k}) = \sqrt{\xi_j^2(\mathbf{k}) + |\Delta_j(\mathbf{k})|^2}$ with $\Delta_j(\mathbf{k}) = \Delta_{j0}\Gamma_j(\mathbf{k})$. When both $|\Delta_{10}|$ and $|\Delta_{20}|$ are non-zero, $E_j(\mathbf{k})$ is always gapped. This gap can be indirect BCS-like, that is, at non-zero momentum; or direct BEC-like, that is, at zero momentum. Spectroscopically, there are three regions: I) where $\mu > \varepsilon_0$ and both $E_1(\mathbf{k})$ and $E_2(\mathbf{k})$ have indirect BCS-like gaps (BCS-BCS); II) where $\varepsilon_0 > \mu > 0$ and $E_1(\mathbf{k})$ has an indirect BCS-like gap and $E_2(\mathbf{k})$ has a direct BEC-like gap (BCS-BEC); and III) where $\mu < 0$ and both $E_1(\mathbf{k})$ and $E_2(\mathbf{k})$ have direct BEC-like gaps (BEC-BEC).

While Ω_c depends only on the moduli $|\Delta_{j0}|$, we can write Ω_p in terms of the modulus and phase of $\Delta_{j0} = |\Delta_{j0}| \exp(i\varphi_j)$ to obtain $\Omega_p = -g_{11}|\Delta_{10}|^2 - g_{22}|\Delta_{20}|^2 - 2g_{12}|\Delta_{10}||\Delta_{20}| \cos\delta\varphi$, where $\delta\varphi = \varphi_2 - \varphi_1$ is the relative phase between the two order parameters. Here, $g_{11} = -V_{22}/\det\mathbf{V}$, $g_{22} = -V_{11}/\det\mathbf{V}$, and $g_{12} = -V_{12}/\det\mathbf{V}$ with $\det\mathbf{V} = (V_{11}V_{22} - V_{12}V_{21}) > 0$. Since $V_{12} = V_{21} = -J$, $g_{12} = J/\det\mathbf{V}$ defines the sign of the prefactor of $\cos\delta\varphi$. When $|\Delta_{10}|$ and $|\Delta_{20}|$ are non-zero and $J > 0$ ($J < 0$), the thermodynamic potential Ω is minimized when the phases of the order parameters are the same (differ by π), that is, $\varphi_2 = \varphi_1$ ($\varphi_2 = \varphi_1 \pm \pi$). When $J = 0$, φ_1 and φ_2 are completely independent. This means that the limit $J \to 0$ is singular, and switching $J \to -J$ while keeping $V_{11}, V_{22}, \varepsilon_0$, and μ fixed at any values leads to a 0-π QPT.

From the condition $\delta\Omega/\delta\Delta_{i0}^* = 0$, we get the order parameter equations

$$\Delta_{i0} = -\sum_{j\mathbf{k}} V_{ij} \frac{\Delta_{j0}|\Gamma_j(\mathbf{k})|^2}{2E_j(\mathbf{k})} \tanh\left[\frac{\beta E_j(\mathbf{k})}{2}\right]. \tag{2}$$

The number equation is $N = -\partial\Omega/\partial\mu|_{T,V}$, leading to $N = N_1 + N_2$, where $N_j = 2\sum_{\mathbf{k}} n_j(\mathbf{k})$ is the number of particles in band j, and $n_j(\mathbf{k}) = \frac{1}{2}\left\{1 - \frac{\xi_j(\mathbf{k})}{E_j(\mathbf{k})} \tanh\left[\frac{\beta E_j(\mathbf{k})}{2}\right]\right\}$ is the momentum distribution for each internal (spin) state. For $J > 0$ with $\varphi_1 = \varphi_2$ or $J = 0$ with φ_1 and φ_2 being independent, we obtain $|\Delta_{j0}|$ and μ from the order parameter and number equations by writing $V_{11} = -|V_{11}|$ and $V_{22} = -|V_{22}|$ in terms of the s-wave scattering lengths a_{s_j} [30] via $\frac{1}{|V_{jj}|} = -\frac{m_j L^3}{4\pi a_{s_j}} + \sum_{\mathbf{k}} \frac{|\Gamma_j(\mathbf{k})|^2}{2\varepsilon_j(\mathbf{k})}$. We use the total particle density $n = N/V$ to define an effective Fermi momentum k_F via $n = k_F^3/3\pi^2$ and an effective Fermi energy $\varepsilon_F = k_F^2/2m$ as momentum and energy scales, since we choose $m_1 = m_2 = m$ from now on. Note that $k_F^3 = k_{F_1}^3 + k_{F_2}^3$. In fig. 2, we show $|\Delta_{10}|/\varepsilon_F$ and $|\Delta_{20}|/\varepsilon_F$ *vs.* $1/k_F a_{s_2}$ for fixed $1/k_F a_{s_1} = -1.5$, but different values of $(\varepsilon_0/\varepsilon_F, J/\varepsilon_F)$. Note that in panels (a) and (b), where $J/\varepsilon_F \neq 0$, both bands are always superfluid with $|\Delta_{10}|/\varepsilon_F \neq 0$ and $|\Delta_{20}|/\varepsilon_F \neq 0$. In panels (c) and (d), where $J/\varepsilon_F = 0$, there are regions where both bands are superfluid with $|\Delta_{10}|/\varepsilon_F \neq 0$ and $|\Delta_{20}|/\varepsilon_F \neq 0$. But when

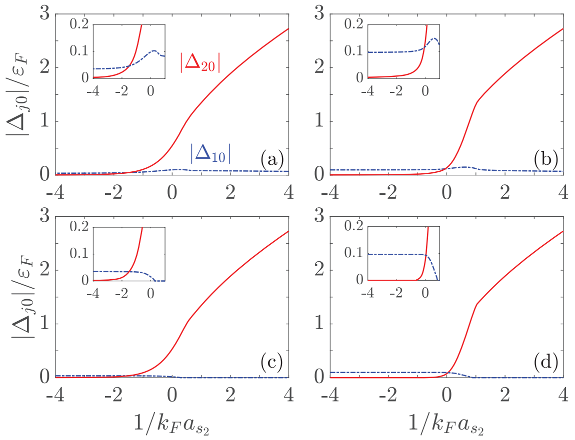

Fig. 2: Order parameters $|\Delta_{10}|/\varepsilon_F$ (dot-dashed blue lines) and $|\Delta_{20}|/\varepsilon_F$ (solid red lines) *vs.* $1/k_F a_{s_2}$ for fixed $1/k_F a_{s_1} = -1.5$ and different values of $(\varepsilon_0/\varepsilon_F, J/\varepsilon_F)$: (a) $(0, 10^{-3})$; (b) $(0.9, 10^{-3})$; (c) $(0, 0)$; (d) $(0.9, 0)$. Insets show $|\Delta_{j0}|/\varepsilon_F$ for $-4 \le 1/k_F a_{s_2} \le 1$.

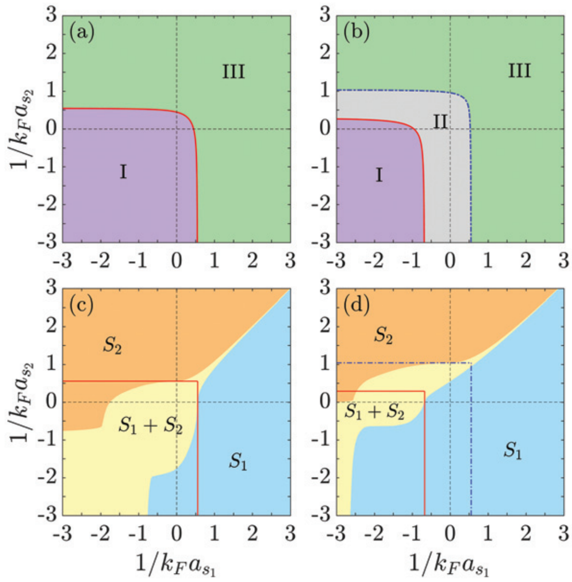

Fig. 3: Phase diagrams in $1/k_F a_{s_1}$ *vs.* $1/k_F a_{s_2}$ plane for different values of $(\varepsilon_0/\varepsilon_F, J/\varepsilon_F)$: (a) $(0, 10^{-3})$; (b) $(0.9, 10^{-3})$; (c) $(0, 0)$; (d) $(0.9, 0)$. In (a) and (b): the BCS-BCS region (I, purple), BCS-BEC region (II, gray), and BEC-BEC region (III, green) are shown; the solid red line is for $\mu = \varepsilon_0 = 0$. In (c) and (d): three phases of S_1+S_2 (yellow) with $|\Delta_{10}|, |\Delta_{20}| \neq 0$, S_1 (blue) with $|\Delta_{10}| \neq 0$ and $|\Delta_{20}| = 0$, and S_2 (orange) with $|\Delta_{10}| = 0$ and $|\Delta_{20}| \neq 0$ are depicted; the vertical solid red (dotdahed blue) is for $\mu = \varepsilon_0 = 0.9\varepsilon_F$ $(\mu = 0)$.

$1/k_F a_{s_2}$ is sufficiently large, only band 2 is superfluid as $|\Delta_{10}|/\varepsilon_F = 0$ and $|\Delta_{20}|/\varepsilon_F \neq 0$.

The ground-state phase diagrams in the $1/k_F a_{s_1}$ *vs.* $1/k_F a_{s_2}$ plane, shown in fig. 3, are determined by analyzing $|\Delta_{10}|$, $|\Delta_{20}|$, and μ. The solid red (dot-dashed blue) line corresponds to $\mu = \varepsilon_0$ $(\mu = 0)$. In panels (a) and (b), where $J/\varepsilon_F \neq 0$, superfluidity arises in both bands for all values of $1/k_F a_{s_1}$ and $1/k_F a_{s_2}$ as $|\Delta_{10}|$ and $|\Delta_{20}|$ are always non-zero. Thus, there are only crossovers between spectroscopically different superfluids phases: I) BCS-BCS (purple) with $\mu > \varepsilon_0$, II) BCS-BEC (gray) with $\varepsilon_0 > \mu > 0$, and III) BEC-BEC (green) with $\mu < 0$. However, in panels (c) and (d), where $J/\varepsilon_F = 0$, there are three different phases and QPTs between them. The phases are S_1 (blue) with $|\Delta_{10}| \neq 0$ and $|\Delta_{20}| = 0$, S_2 (orange) with $|\Delta_{10}| = 0$ and $|\Delta_{20}| \neq 0$, and $S_1 + S_2$ (yellow) with $|\Delta_{10}| \neq 0$ and $|\Delta_{20}| \neq 0$. For $J/\varepsilon_F = 0$, there is no superfluid proximity effect, thus, the strongest-coupled band depletes the weakest-coupled band forcing the order parameter of the latter to zero. At the boundaries between $S_1 + S_2$ and S_1 (S_2), $|\Delta_{20}|$ $(|\Delta_{10}|)$ vanishes and the transitions are continuous. Furthermore, for $J/\varepsilon_F = 0$, sufficiently large $1/k_F a_{s_1}$ $(1/k_F a_{s_2})$, and one of the bands in its normal phase $|\Delta_{20}| = 0$ $(|\Delta_{10}|) = 0$, the particle number N_2 (N_1) vanishes when $\mu < \varepsilon_0$ $(\mu < 0)$. This is a trivial situation, where all particles are paired in band 1 (band 2) and no free particles are present in band 2 (band 1). These calculations confirm previous conjectures [29] and shine light on earlier works that missed the full phase diagrams containing double crossovers and QPTs [31,42–46].

To characterize further the spectroscopic regions (I), II), III)) and the QPTs for $J/\varepsilon_F = 0$, we discuss the pair sizes ξ_j within the j-th band [19,47]:

$$\xi_j^2 = \left(\sum_{\mathbf{k}} \phi_j^*(\mathbf{k}) \left[-\nabla^2_{\mathbf{k}} \right] \phi_j(\mathbf{k}) \right) \Big/ \sum_{\mathbf{k}} |\phi_j(\mathbf{k})|^2, \qquad (3)$$

where $\phi_j(\mathbf{k}) = \Delta_j(\mathbf{k})/2E_j(\mathbf{k})$ is the non-normalized pair wave function. In fig. 4, we show $k_F\xi_1$ (dot-dashed blue line) and $k_F\xi_2$ (solid red line) *vs.* scattering parameter $1/k_F a_{s_2}$ for fixed $1/k_F a_{s_1} = -1.5$ and different values of $(\varepsilon_0/\varepsilon_F, J/\varepsilon_F)$. Panels (a) and (b) show that when J/ε_F is sufficiently large, *e.g.*, $J/\varepsilon_F = 10^{-3}$, the pair sizes always decrease as $1/k_F a_{s_2}$ increases. Thus, $k_F\xi_j$ monotonically decreases from a BCS-BCS region I) to a BEC-BEC region III) in (a), and monotonically decreases from a BCS-BCS region I) to a BCS-BEC region II) to a BEC-BEC region III) in (b). Panels (c) and (d) show that, for a smaller $J/\varepsilon_F = 10^{-4}$, $k_F\xi_1$ continues to decrease monotonically with $1/k_F a_{s_2}$, however $k_F\xi_2$ first increases and then decreases before entering the BEC-BEC region III). This non-monotonic behavior of $k_F\xi_2$ is simply a reflection of the proximity to a QPT, where the order parameter $|\Delta_{20}|$ is approaching zero. The emergence of two QPTs is shown in panels (e) and (f), where $J/\varepsilon_F = 0$. In this case, $k_F\xi_1$ $(k_F\xi_2)$ increases (decreases) monotonically with $1/k_F a_{s_2}$ and is zero in the orange S_2 (blue S_1) region. The divergence in $k_F\xi_j$ occurs as $|\Delta_{j0}| \to 0$.

Ginzburg-Landau theory. – As shown in fig. 3, QPTs occur only for $J/\varepsilon_F = 0$. In the vicinity of the phase boundaries between the $S_1 + S_2$ (yellow) and S_1 (blue) or S_2 (orange) phases, a Ginzburg-Landau (GL) theory is possible. Writing the order parameter as $\Delta_j(\mathbf{q}) = |\Delta_{j0}|\delta_{\mathbf{q},0} + \Lambda_j(\mathbf{q})$, and setting $|\Delta_{j0}| = 0$ at the appropriate

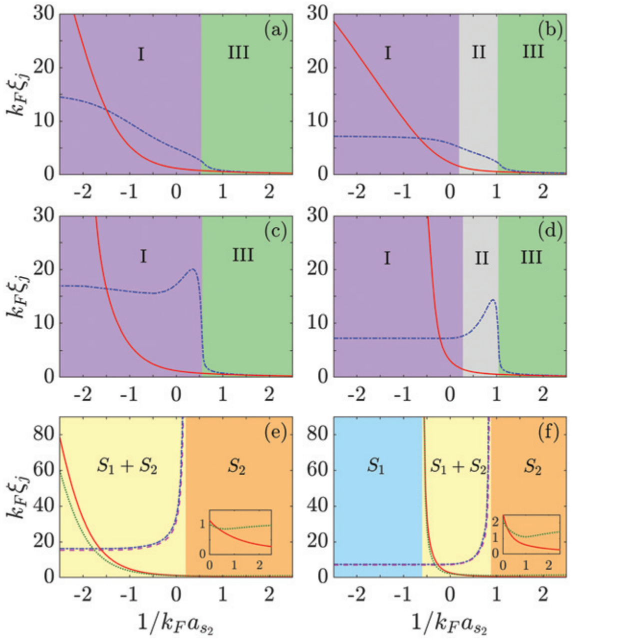

Fig. 4: Pair sizes $k_F\xi_1$ (dot-dashed blue line) and $k_F\xi_2$ (solid red line) *vs.* $1/k_Fa_{s_2}$ for fixed $1/k_Fa_{s_1} = -1.5$ and different values of $(\varepsilon_0/\varepsilon_F, J/\varepsilon_F)$: (a) $(0, 10^{-3})$; (b) $(0.9, 10^{-3})$; (c) $(0, 10^{-4})$; (d) $(0.9, 10^{-4})$; (e) $(0, 0)$; (f) $(0.9, 0)$. Background color are as in fig. 3. The value $k_F\xi_j = 1$ approximately separates the BCS-like ($k_F\xi_j \gg 1$) and BEC-like ($k_F\xi_j \ll 1$) regimes. The coherence lengths $k_F\xi_{1c}$ (dashed magenta line) and $k_F\xi_{2c}$ (dotted green line) are shown in panels (e) and (f). Insets in (e) and (f) compare pair size $k_F\xi_2$ (solid red) and coherence length $k_F\xi_{2c}$ (dotted green).

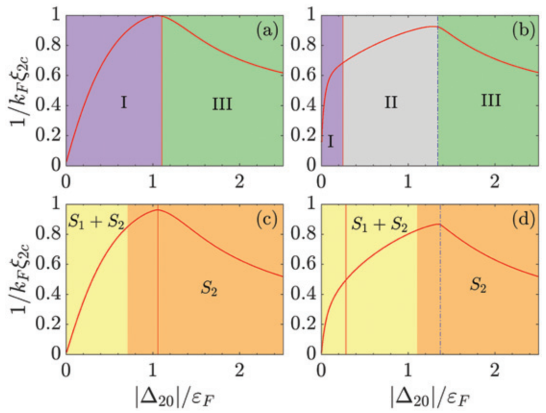

Fig. 5: The coherence length parameter $1/k_F\xi_{2c}$ (solid red lines) at fixed $1/k_Fa_{s_1} = -1.5$ as $1/k_Fa_{s_2}$ changes from -4.0 to 3.5 for different values of $(\varepsilon_0/\varepsilon_F, J/\varepsilon_F)$: (a) $(0, 10^{-3})$; (b) $(0.9, 10^{-3})$; (c) $(0, 0)$; (d) $(0.9, 0)$. Background colors are as in fig. 3. In (a) and (c) the vertical solid red line is for $\mu = \varepsilon_0 = 0$, while in (b) and (d) the vertical solid red (dot-dahed blue) is for $\mu = \varepsilon_0 = 0.9\varepsilon_F$ ($\mu = 0$).

boundary, the GL thermodynamic potential becomes

$$\Omega_{\rm GL} = \Omega_i + \Omega_{jN} + \int \frac{{\rm d}^3\mathbf{r}}{L^3}\left[\Lambda_j^*(\mathbf{r}) M_j(\hat{\mathbf{q}})\Lambda_j(\mathbf{r}) + b_j|\Lambda_j(\mathbf{r})|^4\right],$$

where Ω_i (Ω_{jN}), with $i \neq j$, is the thermodynamic potential of band i (j) which remains superconducting (becomes normal) at the phase boundary. The fluctuation terms under the integral are $M_j(\hat{\mathbf{q}}) = a_j + c_j\hat{\mathbf{q}}^2/2m_j$, and $b_j > 0$. The GL coherence length ξ_{jc} for pairing in the j-th band is $\xi_{jc}^2 = c_j/2m_ja_j$, where $a_j = M_j(\mathbf{0})$ and $c_j = 2m_j\left[\partial^2 M_j(\mathbf{q})/\partial\mathbf{q}^2\right]_{\mathbf{q}=\mathbf{0}}$, with

$$M_j(\mathbf{q}) = -g_{jj} - \sum_{\mathbf{k},\lambda} |\Gamma(\mathbf{k})|^2 \alpha_j^{p\lambda}(\mathbf{k}_+, \mathbf{k}_-)\beta_j^{p\lambda}(\mathbf{k}_+, \mathbf{k}_-),$$

and $\mathbf{k}_\pm = \mathbf{k} \pm \mathbf{q}/2$. The index $\lambda = \{p, h\}$ represents quasiparticle (p) or quasihole (h) contributions. The functions within the sum are

$$\alpha_j^{p\lambda}(\mathbf{k}_+, \mathbf{k}_-) = \frac{\tanh\left[E_j(\mathbf{k}_+)/2T\right] \pm \tanh\left[E_j(\mathbf{k}_-)/2T\right]}{E_j(\mathbf{k}_+) \pm E_j(\mathbf{k}_-)},$$

with the $+$ ($-$) sign being for $\lambda = p$ ($\lambda = h$), and

$$\beta_j^{p\lambda}(\mathbf{k}_+, \mathbf{k}_-) = \frac{1}{4}\left[1 \pm \frac{\xi_j(\mathbf{k}_+)\xi_j(\mathbf{k}_-)}{E_j(\mathbf{k}_+)E_j(\mathbf{k}_-)}\right]$$

are the coherence factors. Setting $|\Delta_{j0}| \to 0$ at the appropriate phase boundary leads to $\xi_{jc} = \xi_{j0}|\eta_j - \eta_j^*|^{-1/2}$ at $T = 0$, where $\eta_j = 1/k_Fa_{s_j}$ and $\eta_j^* = 1/k_Fa_{s_j}^*$ is the critical interaction parameter. When corresponding phase boundaries are crossed, ξ_{jc} diverges similarly to the pair size ξ_j, signaling continuous phase transitions over all phase boundaries in the $1/k_Fa_{s_1}$ *vs.* $1/k_Fa_{s_2}$ plane. This is illustrated in panels (e) and (f) of fig. 4, where it is shown that in the BEC regime ($1/k_Fa_{s_2} \to \infty$), the pair size $k_F\xi_2 \to 0$, while the coherence length $k_F\xi_{2c} \to C \neq 0$. We emphasize that the GL coherence length ξ_{jc} and the pair size ξ_j have different physical meanings. The former is a measure of the phase coherence length of the superfluid and the latter is a measure of the size of Cooper pairs.

We describe next, the relation between ξ_{jc} and $|\Delta_{j0}|$. In fig. 5, we show the coherence length parameter $1/k_F\xi_{2c}$ *vs.* $|\Delta_{20}|$ along a straight line path in interaction parameter space with $1/k_Fa_{s_1} = -1.5$ and $1/k_Fa_{s_2}$ changing from -4.0 to 3.5 for fixed values of band offset ε_0 and Josephson coupling J. The parameters $(\varepsilon_0/\varepsilon_F, J/\varepsilon_F)$ are: (a) $(0, 10^{-3})$; (b) $(0.9, 10^{-3})$; (c) $(0, 0)$; and (d) $(0.9, 0)$. Panels (a) and (b) represent crossovers, while panels (c) and (d) represent QPTs. Notice that in (a) and (b) the coherence length ξ_{2c} never diverges, so $1/k_F\xi_{2c}$ is never zero, because there are only crossovers. A similar behavior for ξ_{1c} *vs.* $|\Delta_{10}|$ also occurs (not shown). However, in (c) and (d) ξ_{2c} diverges ($1/k_F\xi_{2c} = 0$) at the $S_1/(S_1 + S_2)$ boundary, where $|\Delta_{20}| = 0$. A divergence in ξ_{1c} ($1/k_F\xi_{1c} = 0$), not shown, also occurs at the $(S_1 + S_2)/S_2$ boundary, where $|\Delta_{10}| = 0$. In all panels, $1/k_F\xi_{2c}$ is linear in $|\Delta_{20}|/\varepsilon_F$ for $|\Delta_{20}|/\varepsilon_F \ll 1$, reflecting the BCS relation $k_F\xi_{2c} \propto \varepsilon_F/|\Delta_{20}|$. Notice also that $1/k_F\xi_{2c}$ exhibits a maximum in all panels, that is, $k_F\xi_{2c}$ has a minimum, which is located at $\mu = \varepsilon_0 = 0$ (vertical solid red line) in (a) and (c), and located at $\mu = 0$ (vertical dot-dashed blue line) in (b) and (d). The maxima, where $1/k_F\xi_{2c} \sim \mathcal{O}(1)$, occurs effectively for $\mu = \varepsilon_0$ when falls below the bottom of band 2, and the gap in the quasiparticle excitation spectrum changes qualitatively from indirect to direct. This observation generalizes and clarifies the special role that $1/k_F\xi_{jc}$ plays not only in the BCS-BEC crossovers, like in the one-band case [11,47–49], but also in QPTs.

Thermodynamic signatures. – Next, we discuss the ground-state (zero-temperature) dimensionless compressibility $\widetilde{\alpha} = \partial N/\partial\widetilde{\mu}|_{T,V}$, which is directly related to the dimension-full compressibility $\kappa = \partial n/\partial\mu|_{T,V}/n^2$, where $n = N/V$ is the total density and V is the volume. Notice that $\widetilde{\alpha} = \widetilde{\alpha}_1 + \widetilde{\alpha}_2$, where $\widetilde{\alpha}_j = \partial N_j/\partial\widetilde{\mu}|_{T,V}$ is the compressibility of the j-th band.

In fig. 6, we show $\widetilde{\alpha}/N$ *vs.* $1/k_Fa_{s_2} \in (-3, 3)$ with $1/k_Fa_{s_1} = -1.5$ for fixed values of band offset ε_0 and Josephson coupling J. The dotted black curve is the total $\widetilde{\alpha}/N$, the dot-dashed blue curve is the contribution $\widetilde{\alpha}_1/N$ from band 1, the solid red curve is the contribution $\widetilde{\alpha}_2/N$ from band 2. The parameters $(\varepsilon_0/\varepsilon_F, J/\varepsilon_F)$ are: (a) $(0, 10^{-3})$; (b) $(0.9, 10^{-3})$; (c) $(0, 0)$; and (d) $(0.9, 0)$. Panels (a) and (b) represent crossovers, while panels (c) and (d) represent QPTs. Notice that in (a) and (b) the only interesting feature in the compressibility is the minimum that occurs near the crossover line between regions I) and II) in (a) and between regions II) and III) in (b), where the number of particles N_1 in band 1 gets nearly depleted by the strong interactions in band 2. It is important to mention that N_1 does not vanish at finite $1/k_Fa_{s_2}$ because $J/\varepsilon_F = 10^{-3} \neq 0$, but it does vanish at asymptotically large $1/k_Fa_{s_2}$, that is, when $1/k_Fa_{s_2} \to \infty$. The minimum in panels (c) and (d), where $J = 0$, develops a cusp because N_1 vanishes at $\mu = 0$, being completely depleted by the strong interactions in band 2. As a result, the compressibility $\widetilde{\alpha}_1$ is strictly zero at that point and beyond. This is a trivial case, where there are no normal fermions in band 1, and is not related to any QPTs where superfluid phases disappear. Panels (c) and (d) show that the compressibility $\widetilde{\alpha}/N$ has small discontinuities at the phase boundaries. In (c), $\widetilde{\alpha}_1/N$ has a discontinuity at the $(S_1 + S_2)/S_2$ boundary, where $|\Delta_{10}|$ vanishes, as seen in the inset. In (d), discontinuities occur in $\widetilde{\alpha}_1/N$ at the $(S_1 + S_2)/S_2$ boundary, where $|\Delta_{10}| = 0$ and in $\widetilde{\alpha}_2/N$ at the $S_1/(S_1 + S_2)$ boundary, where $|\Delta_{20}| = 0$, as shown in the insets. The small discontinuities show an increase of the compressibility as a new superfluid phase is entered. The analytical expression for the jump $\Delta\widetilde{\alpha}_j/N = \widetilde{\alpha}_j/N|_{\text{sup}} - \widetilde{\alpha}_j/N|_{\text{nor}}$ at the critical points $\mu = \mu_c$ is

$$\frac{\Delta\widetilde{\alpha}_j}{N} = S_{jc} - \frac{3}{2}\widetilde{\mu}_{jc}^{-1/2}, \qquad (4)$$

where $\widetilde{\mu}_{1c} = \widetilde{\mu}_c = \mu_c/\varepsilon_F$ and $\widetilde{\mu}_{2c} = \widetilde{\mu}_c - \widetilde{\varepsilon}_0$ with $\widetilde{\varepsilon}_0 = \varepsilon_0/\varepsilon_F$. The contribution from the superconducting side is $S_{jc} = L_{jc}M_{jc}$, where the first term is $L_{jc} = (1/2N)\sum_{\mathbf{k}} |\Gamma_j(\mathbf{k})|^2 \left\{\text{sgn}\left[\widetilde{\xi}_{jc}(\mathbf{k})\right]/|\widetilde{\xi}_{jc}(\mathbf{k})|^2\right\}$, and the second is

$$M_{jc} = \frac{\sum_{\mathbf{k}} |\Gamma_j(\mathbf{k})|^2 \text{sgn}\left[\widetilde{\xi}_{jc}(\mathbf{k})\right]/2|\widetilde{\xi}_{jc}(\mathbf{k})|^2}{\sum_{\mathbf{k}} |\Gamma_j(\mathbf{k})|^4/4|\widetilde{\xi}_{jc}(\mathbf{k})|^3},$$

with $\widetilde{\xi}_{jc}(\mathbf{k}) = \widetilde{\varepsilon}_j(\mathbf{k}) - \widetilde{\mu}_c$. Discontinuities in insets of fig. 6(c), (d) are small, but get bigger as phase boundaries are crossed for larger values of $1/k_Fa_{s_1}$.

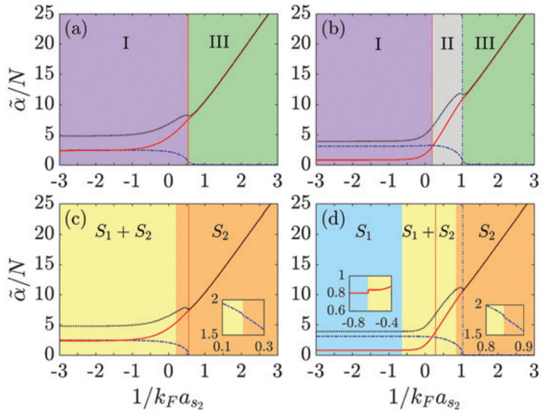

Fig. 6: Dimensionless compressibility $\widetilde{\alpha} = \partial N/\partial\widetilde{\mu}|_{T,V}$ (dotted black line) *vs.* $1/k_Fa_{s_2}$ for fixed $1/k_Fa_{s_1} = -1.5$ and different values of $(\varepsilon_0/\varepsilon_F, J/\varepsilon_F)$: (a) $(0, 10^{-3})$; (b) $(0.9, 10^{-3})$; (c) $(0, 0)$; (d) $(0.9, 0)$. The dot-dashed blue curves show the contribution $\widetilde{\alpha}_1$ of band 1, and the solid red curves show the contibution $\widetilde{\alpha}_2$ of band 2. Background colors are as in fig. 3. In (a) and (c) the vertical solid red line is for $\mu = \varepsilon_0 = 0$, while in (b) and (d) the vertical solid red (dot-dahed blue) is for $\mu = \varepsilon_0 = 0.9\varepsilon_F$ ($\mu = 0$).

Conclusions. – We showed that, during the evolution from BCS to BEC superfluidity, elusive quantum phase transitions (QPTs) occur by tuning s-wave interactions and band offset in two-band superfluids. This is in sharp contrast with single-band s-wave systems where only a crossover is possible. Our results may bypass long-standing experimental difficulties in the search of QPTs for ultracold fermions with one-band, where at least p-wave pairing is required, but unfortunately p-wave Cooper pairs are currently short-lived. In addition to QPTs, we have also established three spectroscopically distinct superfluid regions —I) BCS-BCS, II) BCS-BEC, and III) BEC-BEC— possessing crossovers between them, where pair sizes from each band can be dramatically different. We analyzed pair sizes and coherence lengths, within the Ginzburg-Landau theory, and showed that they diverge at the appropriate phase boundaries. We also characterized the QPTs thermodynamically, by demonstrating the existence of discontinuities in the compressibility as phase boundaries are crossed. Lastly, our results may motivate the experimental search for multiband superfluidity and QPTs in ultracold such as ^{6}Li, ^{40}K, ^{87}Sr, and ^{173}Yb.

* * *

We thank the National Natural Science Foundation of China (Grants 11774425 and 12074428), the Beijing Natural Science Foundation (Grant Z180013), and the National Key R&D Program of China (Grant 2018YFA0306501) for financial support.

Data avaliability statement: All data support the findings of this study are included within the article (and any supplementary files).

REFERENCES

[1] Sobirey L., Luick N., Bohlen M., Biss H., Moritz H. and Lompe T., *Science*, **372** (2021) 844.
[2] Del Pace G., Kwon W. J., Zaccanti M., Roati G. and Scazza F., *Phys. Rev. Lett.*, **126** (2021) 055301.
[3] Kuhn C. C. N., Hoinka S., Herrera I., Dyke P., Kinnunen J. J., Bruun G. M. and Vale C. J., *Phys. Rev. Lett.*, **124** (2020) 150401.
[4] Kagan M. Yu. and Turlapov A. V., *Phys.-Usp.*, **62** (2019) 215.
[5] Richie-Halford A., Drut J. E. and Bulgac A., *Phys. Rev. Lett.*, **125** (2020) 060403.
[6] Zhou H. and Ma Y., *Sci. Rep.*, **11** (2021) 1228.
[7] Ebling U., Alavi A. and Brand J., *Phys. Rev. Res.*, **3** (2021) 023142.
[8] Kurkjian H., Klimin S. N., Tempere J. and Castin Y., *Phys. Rev. Lett.*, **122** (2019) 093403.
[9] Leggett A. J., *J. Phys. Colloq.*, **41** (1980) 7.
[10] Nozières P. and Schmitt-Rink S., *J. Low Temp. Phys.*, **59** (1985) 195.
[11] Sá de Melo C. A. R., Randeria M. and Engelbrecht J. R., *Phys. Rev. Lett.*, **71** (1993) 3202.
[12] Sá de Melo C. A. R., *Phys. Today*, **61** (2008) 45.
[13] Nakagawa Y., Kasahara Y., Nomoto T., Arita R., Nojima T. and Iwasa Y., *Science*, **372** (2021) 190.
[14] Park J. M., Cao Y., Watanabe K., Taniguchi T. and Jarillo-Herrero P., *Nature*, **590** (2021) 249.
[15] Greiner M., Regal C. A. and Jin D. S., *Nature (London)*, **426** (2003) 537.
[16] Jochim S., Bartenstein M., Altmeyer A., Hendl G., Riedl S., Chin C., Hecker Denschlag J. and Grimm R., *Science*, **302** (2003) 2101.
[17] Strecker K. E., Partridge G. B. and Hulet R. G., *Phys. Rev. Lett.*, **91** (2003) 080406.
[18] Zwierlein M. W., Stan C. A., Schunck C. H., Raupach S. M. F., Gupta S., Hadzibabic Z. and Ketterle W., *Phys. Rev. Lett.*, **91** (2003) 250401.
[19] Duncan R. D. and Sá de Melo C. A. R., *Phys. Rev. B*, **62** (2000) 9675.
[20] Botelho S. S. and Sá de Melo C. A. R., *Phys. Rev. B*, **71** (2005) 134507.
[21] Read N. and Green D., *Phys. Rev. B*, **61** (2000) 10267.
[22] Botelho S. S. and Sá de Melo C. A. R., *J. Low Temp. Phys.*, **140** (2005) 409.
[23] Gaebler J. P., Stewart J. T., Bohn J. L. and Jin D. S., *Phys. Rev. Lett.*, **98** (2007) 200403.
[24] Fuchs J., Ticknor C., Dyke P., Veeravalli G., Kuhnle E., Rowlands W., Hannaford P. and Vale C. J., *Phys. Rev. A*, **77** (2008) 053616.
[25] Inada Y., Horikoshi M., Nakajima S., Kuwata-Gonokami M., Ueda M. and Mukaiyama T., *Phys. Rev. Lett.*, **101** (2008) 100401.
[26] Iskin M. and Sá de Melo C. A. R., *Phys. Rev. A*, **74** (2006) 013608.
[27] Chang Y.-T, Senaratne R., Cavazos-Cavazos, D. and Hulet R. G., *Phys. Rev. Lett.*, **125** (2020) 263402.
[28] Marcum A. S., Fonta F. R., Ismail A. M. and O'hara K. M., arXiv:2007.15783 (2007).
[29] Sá de Melo C. A. R., in *Erice Summer School, Multi-Condensates Superconductivity* (Superstripes Press, Rome) 2014, p. 27.
[30] Iskin M. and Sá de Melo C. A. R., *Phys. Rev. B*, **72** (2005) 024512.
[31] Iskin M. and Sá de Melo C. A. R., *Phys. Rev. B*, **74** (2006) 144517.
[32] Guidini A. and Perali A., *Supercond. Sci. Technol.*, **27** (2014) 124002.
[33] Wolf S., Vagov A., Shanenko A. A., Axt V. M., Perali A. and Albino Aguiar J., *Phys. Rev. B*, **95** (2017) 094521.
[34] Salasnich L., Shanenko A. A., Vagov A., Albino Aguiar J. and Perali A., *Phys. Rev. B*, **100** (2019) 064510.
[35] Tajima H., Yerin Y., Perali A. and Pieri P., *Phys. Rev. B*, **99** (2019) 180503.
[36] DeSalvo B. J., Yan M., Mickelson P. G., Martinez de Escobar Y. N. and Killian T. C., *Phys. Rev. Lett.*, **105** (2010) 030402.
[37] Stellmer S., Grimm R. and Schreck F., *Phys. Rev. A*, **84** (2011) 043611.
[38] Fukuhara T., Takasu Y., Kumakura M. and Takahashi Y., *Phys. Rev. Lett.*, **98** (2007) 030401.
[39] Kitagawa M., Enomoto K., Kasa K., Takahashi Y., Ciuryło R., Naidon P. and Julienne P. S., *Phys. Rev. A*, **77** (2008) 012719.
[40] Höfer M., Riegger L., Scazza F., Hofrichter C., Fernandes D. R., Parish M. M., Levinsen J., Bloch I. and Fölling S., *Phys. Rev. Lett.*, **115** (2015) 265302.
[41] Pagano G., Mancini M., Cappellini G., Livi L., Sias C., Catani J., Inguscio M. and Fallani L., *Phys. Rev. Lett.*, **115** (2015) 265301.
[42] Yerin Y., Tajima H., Pieri P. and Perali A., *Phys. Rev. B*, **100** (2019) 104528.
[43] Komendová L., Chen Y., Shanenko A. A., Milosević M. V. and Peeters F. M., *Phys. Rev. Lett.*, **108** (2012) 207002.
[44] Iskin M. and Sá de Melo C. A. R., *J. Low Temp. Phys.*, **149** (2007) 29.
[45] Silaev M. and Babaev E., *Phys. Rev. B*, **85** (2012) 134514.
[46] Silaev M. and Babaev E., *Phys. Rev. B*, **84** (2011) 094515.
[47] Engelbrecht J. R., Randeria M. and Sá de Melo C. A. R., *Phys. Rev. B*, **55** (1997) 15153.
[48] Pistolesi F. and Strinati G. C., *Phys. Rev. B*, **49** (1994) 6356.
[49] Pistolesi F. and Strinati G. C., *Phys. Rev. B*, **53** (1996) 15168.